Potential Payoff of Fusion between HSI and other Sensors[1]

Su May Hsu[2] and Hsiao-hua Burke
MIT Lincoln Laboratory
244 Wood St. Lexington, Mass. 02420-9108

Abstract

In this paper, two examples of sensor fusion are demonstrated. The first is hyperspectral imaging (HSI) with Synthetic Aperture Radar (SAR) and the other is HSI with high-resolution panchromatic imaging (HPI). HSI and SAR fusion exploits different phenomenologies from distinctly different sensors. HSI and HPI fusion optimizes their superior respective spectral and spatial information. Examples are illustrated using field measurements as well as simulated data. Fusion of SAR and HSI data is established at feature level. The fusion results showed reduced false detection and confirmed target detection in the SAR image with background characterization and material identification from HSI. Fusion of HSI and HPI is shown at both data and feature levels. The combined high-resolution spatial-spectral analysis is illustrated for enhanced target identification.

Key words: Hyperspectral imaging (HSI), Synthetic Aperture Radar (SAR), high-resolution panchromatic imaging (HPI), principal component analysis (PCA), background classification, matched filtering, image sharpening, edge detection.

1 Introduction

Hyperspectral imaging sensors collect data in a three-dimensional image cube. It is resolved in along-track, cross-track and spectral dimensions. It has fine spectral resolutions ($\Delta\lambda \sim 10$ nm), typically in visible to SWIR wavelength region (0.4 – 2.5 μm). For each ground sample distance (GSD) pixel within a hyperspectral image, a continuous spectrum is measured and used to identify materials by their reflectance. But it provides no surface penetrations. Additionally, to maintain required SNR, HSI spatial resolutions are in general coarser than broadband imagery resolutions. Thus there is great potential to enhance the overall HSI system performance if fusion with other remotely sensed data can be accomplished. For example, in the application of counter camouflage, concealment and deception (CC&D), HSI can be used to identify ground coverage and surface material. And a FOPEN SAR (Foliage Penetration Synthetic Aperture Radar) can determine if any threat objects are under concealment. In the surface surveillance application, HSI can be augmented with high-resolution broadband panchromatic images to achieve simultaneous high spectral and spatial resolutions for enhanced target detection and identification.

There have been several examples in which both Synthetic Aperture Radar (SAR) and Hyperspectral Imaging (HSI) systems collected data in support of military operations. Principles of low frequency SAR and Hyperspectral imaging are different and their detection capabilities often compliment each other. FOPEN SAR operates at 20-700 MHz. It penetrates foliage and detects targets under tree canopy, but has significant clutter returns from trees. Hyperspectral imaging, on the other hand, is capable of sub-pixel detection and material identification. Both SAR and HSI systems may suffer substantial false alarm and leakage rates due to respective background clutter. It is expected that a combined SAR and HSI system will greatly enhance the detection and identification performance. It is possible that a combined SAR/HSI system could have the imaging sensors cue each other in joint observations. Potential applications for such fusion include counter camouflage, concealment and deception (CC&D) and surveillance of exposed sites.

Hyperspectral imaging sensors collect image data in hundreds of contiguous narrow spectral bands (~10 nm) with moderate spatial resolutions. In contrast, conventional single band or multi-spectral sensors

[1] This work was sponsored by the Department of Air Force under Contract F19628-00-C-0002. Opinions, interpretations, conclusions and recommendations are those of the authors and not necessarily endorsed by the United States Air Force.

[2] Telephone (781) 981-2920; Fax (781) 981-7271; e-mail sumayhsu@ll.mit.edu

typically image in wide, discrete spectral bands with fine spatial resolutions. If hyperspectral image can be spatially "sharpened" via the broadband high-resolution image, the detection and identification performance is expected to improve further. Currently, there are a number of space-based hyperspectral measurement platforms to be launched in the foreseeable future: NASA's EO-1, Air Force's Warfighter-1 and Navy's NEMO (Naval Earth Map Observer). Onboard these systems there are high-resolution panchromatic imaging (HPI) sensors in addition to HSI sensors, with the linear spatial resolution of 3 to 8 times better. It is important that effective approaches of hyperspectral image fusion with the high-resolution broad-band image be explored to enhance the utility of future HSI data.

In the next section, an example of HSI/SAR fusion is demonstrated. Since HSI and SAR are distinctly different sensors exploiting different phenomenology, fusion of HSI and SAR data is established at feature level. In Section 3, fusion of HSI/HPI is explored. Sharpening of HSI with an HPI is first investigated. Then a combined spatial-spectral analysis is illustrated for enhanced target detection and identification

2 HSI/SAR Fusion

A common data set from Dixie-97 data collect over Vicksburg, Mississippi is used here to demonstrate the framework of SAR/HSI fusion. Both P-3 UWB radar (215-730 MHz) and HYDICE (Hyperspectral Digital Image Collection Experiment, 0.4-2.5 μm in 210 bands) collected data at the site. A sketch of the target site is shown in Figure 1. Targets in the forest background included fabric nets and vehicles. Several fabric nets were populated along the tree line around an open area. One fabric net at the tree line was covering a vehicle. All other nets were either empty or covering non-radar reflecting decoys. In addition, there was one vehicle obscured at the lower right corner of the sketch and another vehicle was partially exposed near the top left corner. The SAR data was collected with a 32^{o} depression angle and a ground sample distance (GSD) of 0.23m x 0.4m. The HSI data was collected at 1.5 km altitude with a nadir viewing geometry and GSD of 0.76m x 1.1m.

For the Dixie data collect, a SAR/HSI fusion strategy is established based on their detection characteristics. SAR and HSI data are first processed separately for detection and terrain classification, respectively. Then co-registration is performed to allow overlay of the images. SAR false alarm from trees are reduced by terrain mapping, detection of concealed targets under nets is verified and detection of partially exposed targets is further confirmed with material identification by HSI. In this section, analysis of the HSI data is first given, followed by illustration of SAR/HSI image co-registration and the fusion results.

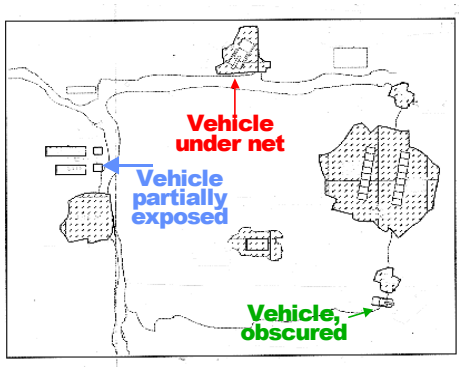

Figure 1 Common data set of SAR/HSI from Dixie data collect, May 1997

2.1 HSI Data Analysis

In order to extract the spectral features leading to further analysis, reduction in spectral dimensionality is applied to the HSI data cube. Principal component transform is used to de-correlate data and maximize the information content in a reduced number of features [1]. Some of the principal components calculated from the HSI data over Dixie are shown in Figure 2. Background classes of open area, trees and roads are apparent in the first and third components. Fabric nets appear with strong contrast to the backgrounds in the seventh component. A matched filter was constructed from the mean of several pixels extracted from the nets. Matched filtering and thresholding are then applied to the HSI data to detect all pixels of fabric

nets. Figure 3 shows the net detection. Result of background mapping of the scene is also included in the figure. Roads, grass, trees and shadow are shown as separate terrain classes. These are results of an unsupervised data clustering operation using the first five principal components.

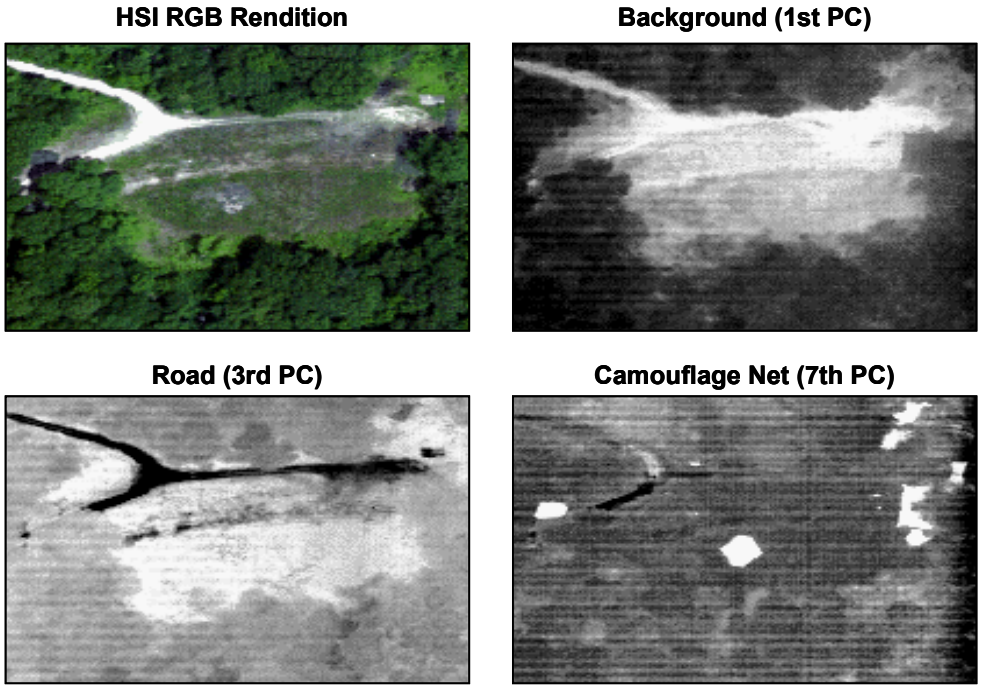

Figure 2 Principal components calculated from the HSI of Dixie data collect

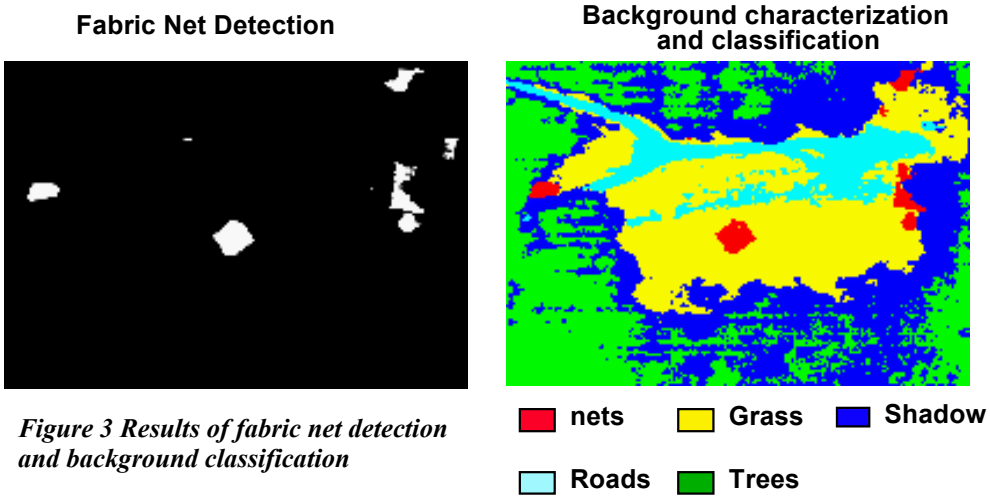

Figure 3 Results of fabric net detection and background classification

2.2 Combined SAR/HSI Analysis and Fusion

To combine SAR and HSI detection results, co-registration is first performed with reference to terrain features such as open and tree areas using scaling, rotation and translation operations. Fusion is then carried out based on the co-registered images. This is illustrated in Figure 4. SAR data is first processed with pixel grouping and thresholding. Target detection on the SAR data is shown on the left. The terrain map derived from HSI data with net detection is depicted in the middle panel of Figure 4. Combining the analyses, only those SAR detections located in either open area or around fabric nets indicated in HSI are

retained. SAR detections that coincide with HSI identifications as trees and are far from open areas or nets are considered false alarms. The combined detection result is shown on the right of the figure. A SAR detection of vehicle appears under a net at the top-right corner. Other nets are empty with no SAR detections. There are several strong SAR detections at the left side of the open area. A spectral angle-mapping algorithm is conducted to match HSI data in the area to our spectral library of paints. Three pixels match well with military gray-tan paint. This indicates the presence of a possible military vehicle and thus confirms the SAR detection.

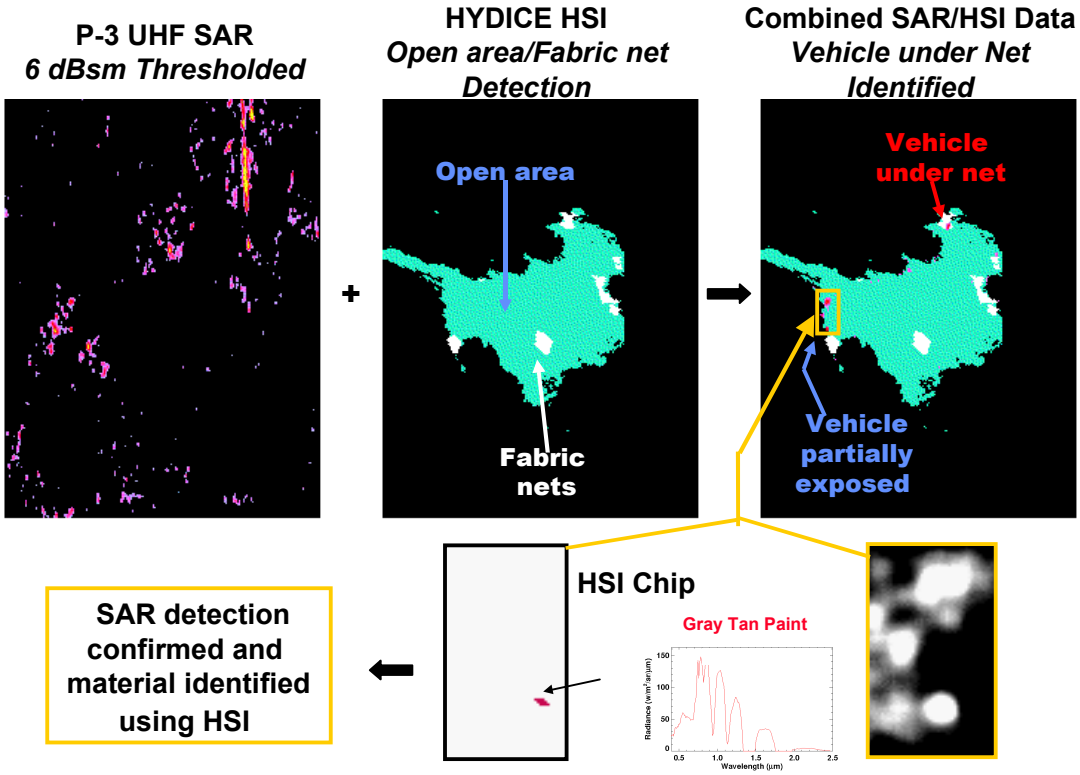

Figure 4 Fusion of SAR and HSI detections

3 HSI/HPI Fusion

A number of image sharpening approaches have been attempted and applied to multi-spectral images (MSI). In this section, three approaches are briefly reviewed and adapted for implementation on HSI. These are the pseudo-inverse technique [2, 3], color normalization and spatial frequency correction methods. In order to demonstrate the sharpening approaches, a sample data is created based on field data. The algorithms are applied to the generated HSI and HPI data for a sharpened HSI. Algorithm performance is then evaluated by comparing with the original truth data. To exploit the full utility potential of combined HSI and HPI data, additional spatial-spectral analysis is also shown for enhanced detection and identification.

3.1 Review and Demonstration of Sharpening Approaches

3.1.1 Pseudo-inverse technique

Given a high-resolution panchromatic image (HPI) co-registered with a set of hyperspectral images, a system of equations can be established for the reconstruction of a high spatial resolution sharpened HSI (SHSI). The value at a pixel in HPI is the spectral sum at the same pixel in SHSI and the spectral value at a pixel in HSI is the pixel-sum over the HSI GSD in the same spectral band of SHSI. If the sharpening ratio

is r and the number of spectral bands is n, then the number of equations over the GSD of HSI is $r^2 + n$, and the number of unknowns for the SHSI reconstruction is $r^2 \times n$. As the sharpening ratio and the number of spectral band increase, the number of unknowns increases faster than the number of additional equations. The system of equations is generally under determined for a unique solution. Pseudo matrix inversion algorithms with least-mean-squared (LMS) estimations are applied to obtain a solution for the fusion problem. The method is described in the following equations:

$$\mathbf{SPI = A^t (A A^t)^{-1} h, \qquad A\ PI = h}$$

Where SPI is an $(n \cdot r^2) \times 1$ array containing pseudo-inverse sharpened HSI values over the GSD of HSI, A is an $(n + r^2) \times (n \cdot r^2)$ matrix of the system equation, $A^t (A A^t)^{-1}$ is the pseudo inverse of A and h is an $(n + r^2) \times 1$ array of the HSI and HPI input values.

In this approach, it is important that the panchromatic image is in perfect registration with HSI. The pseudo inverse technique requires singular value decomposition. In addition, the LMS estimations based on the under determined system of equations may not achieve the required spectral accuracy.

3.1.2 Color Normalization

The color normalization algorithm conventionally used in MSI[4] is modified for HSI sharpening. It multiplies each of the HSI bands by the HPI and the resulting values are each normalized by the averaged HPI data over the number of pixels equivalent to the GSD of HSI. It is defined by the following equation:

$$\mathbf{SCN_i = (HSI_i * HPI) / ave(HPI)_{GSD}}$$

where HSI_i is the HSI band and SCN_i is the sharpened color normalized band.

The approach is straightforward in merging the spatial contrast of HPI into spectral bands of HSI. Similar to the pseudo-inverse technique approach, it also requires precise HSI/HPI registration and the reconstructed data may not achieve great spectral accuracy.

3.1.3 Spatial Frequency Correction

Some sharpening approaches use wavelet transformations [5]. Images are decomposed into different spatial frequency scales. For each of the HSI bands, the high frequency components are replaced with components from HPI. The sharpened image is then obtained via inverse transformation of the modified spectra. In practice, 2-D Fourier transformation can be applied for image spatial frequency analysis. The sharpening process is described as below:

$$\mathbf{SFC_i = FFT^{-1} \{FFT\ (HSI_i)_{low} + FFT(HPI)_{hi}\}}$$

where SFC_i is sharpened HSI_i , FFT $(HSI_i)_{low}$ represents low frequency components of HSI_i and $FFT(HPI)_{hi}$ represents high frequency components of HPI.

In this approach, the spatial shift due to imperfect HSI/HPI registration will show up as a phase shift in the frequency spectrum. In addition, careful selection of the number of high frequency components for replacement is required to avoid artifacts in the sharpened image. Once again, some loss of spectral quality is expected in the reconstructed data.

3.1.4 Demonstration Example

In the three sharpening approaches reviewed, it is indicated that good co-registration between HSI and HPI is required. Since HSI and HPI commonly co-exist on the same platform, co-registration to within a small fraction of an HPI pixel is expected. However, exploration of the registration issue remains an important subject in the ongoing effort for sensor fusion. For performance comparisons, perfect co-registration is assumed here. A set of HSI and HPI is put together and applied with the sharpening methods. A HYDICE (Hyperspectral Digital Image Collection Experiment) major frame is used as the "truth" in both spatial (0.8m/pixel) and spectral ($\Delta\lambda \sim 10$ nm) domains. This input "truth" data is then processed to generate the

contemporaneous test data of HSI (4m/pixel, $\Delta\lambda \sim 10$ nm) and HPI (0.8m/pixel, broad band). The first major frame of HYDICE data from Forest Radiance I Run 05 is used. The frame is a portion of a forest scene. It has 320x320 pixels, 0.8 m per pixel. 25 bands from 0.63 μm to 0.9 μm are used. The HPI data is generated with a 25-band integration. The result is a 320x320 single band image, 0.8 m per pixel. The HSI data is obtained by under-sampling the spatially blurred input data. The FWHM (full width half maximum) of the blurring point spread function (PSF) is 5-pixel wide and the spatial under-sampling is 5 to 1. The resulting HSI has 25 bands; each band is 64x64 pixels in size and 4m per pixel.

Two measures, spectral angle and spectral distance (Euclidean distance), are used to evaluate the sharpening algorithms. These are calculated as:

$$\textbf{Spectral angle (A, B)} = \textbf{COS}^{-1}\textbf{(A . B / |A| |B|)}$$

$$\textbf{Spectral distance (A, B)} = \textbf{|A – B|}$$

Where, A and B are two multi-band spectra.

A zero angle or zero distance represents a perfect match of the two spectra. The sharpened images are compared to the "truth" data in terms of spectral angle and spectral distance. The spectral distance normalized by the pixel amplitude in the truth image is calculated for the fraction of spectral difference. The frame-averaged differences are listed in Table 1. For comparison, the difference measurements from the unsharpened HSI are also included in the table. It shows that the sharpened images improve significantly from the unsharpened HSI in spectral distance, but show no obvious improvement in spectral angle. Among the sharpened images, color normalization (SCN) is closer to the truth in spectral angle than results of pseudo-inverse (SPI) and frequency correction (SFC). On the other hand, the image of frequency correction (SFC) is the closest to the truth in spectral distance. Notice that the comparisons are based on averages over the image. The sharpened images generally appear spatially sharper. However, the impact of such results on target detection and identification is small. Since the combined HSI and HPI data is severely under-determined, spectral features of objects smaller than the original HSI resolution cannot be fully resolved in the reconstruction of the sharpened HSI. For enhanced target detection and identification, additional spatial and spectral analysis at feature level is necessary. In this paper, sharpened HSI image by color normalization will be used for further analysis.

Table 1 Sharpening Algorithm Performance

Average spectral angle and distance over 1st major frame of HYDICE Forest Radiance I Run 05

Performance Metrics	Unsharpened HSI	Sharpened		
		Pseudo Inverse	Frequency Correc.	Color Normal.
Spectral Angle	4.9^o	8.3^o	5.8^o	3.8^o
Spectral Distance	21.6%	13.8%	8.2%	10.0%

3.2 Spatial-spectral Analysis

Various spatial and spectral analysis approaches have been attempted [6,7,8]. Here, a combined spatial-spectral analysis is carried out to demonstrate HSI and HPI fusion for enhanced background characterization and target detection/identification. An analysis approach is depicted in Figure 5. The HSI data is first applied with background classification and anomaly detection. The background class statistics calculated from HSI are employed when the sharpened HSI is also processed with background classification and target detection. At the same time, spatial edge detection for target and background boundaries is applied to the HPI. These edges are combined with results from the sharpened HSI. Targets and backgrounds are spatially defined by the edges. Subsequently, their materials can be identified with spectral characteristics.

In order to evaluate the analysis performance, an expanded data set is used here. Three major frames of HYDICE data from Forest Radiance I Run 05 are used in the demonstration example. The original image

of 300x960 pixels in size, 0.8 m per pixel and 210 bands (the "truth" image) is used as the input. The simulated low-resolution HSI is 60x192 pixels in size, 4 m per pixel and 210 bands. The HPI is obtained with band integration from 0.4 to 0.8 μm, 300x960 pixels with 0.8 m per pixel. A sharpened HSI data cube is constructed from the HSI and HPI with the color normalization method.

Figure 6 shows a reference image (RGB) of HSI, as well as background classification and anomaly detection map derived from the unsharpened HSI. The classification is performed with an unsupervised feature extraction using principal component analysis (PCA) [9]. The Eigen space is first determined for the scene from the covariance matrix of the data cube. It then divides the scene into classes of maximal separations in the Eigen space. In the 5-class classification shown here, road, vegetation (bright and dark), shade and ground are delineated in the scene. The background map and spectral statistics of these classes from HSI are employed in all subsequent processing. Anomalies distinct from backgrounds are also detected. These detections are used to cue for target detection and identification in the combined analysis. Edges are detected from HPI with a SOBEL[10] operator. Overlay of the edges with background classification from sharpened HSI shows better defined background boundaries than in the unsharpened HSI. Spectral matched filtering is applied to sharpened HSI data at regions of anomalies from the earlier HSI data analysis. Spectra of two types of fabric and two types of vehicle paint are employed in the filtering. The results of fabric and vehicle identification are shown in Figure 7. Red and green portions each represent the detection of different vehicle paint. The detections are in general bounded by the edges shown in blue. An enlarged view of the vehicle detections is also shown in the figure. The vehicle size and orientation can be determined from the bounding edges. It is classified as large (4x8 m^2) in size if it is 4 to 6 pixels wide and 8 to 11 pixels long or as small (3x6 m^2) in size if it is 2 to 5 pixels wide and 6 to 9 pixels long. The colored bar next to each vehicle in the enlarged image depicts its type of paint, size and orientation.

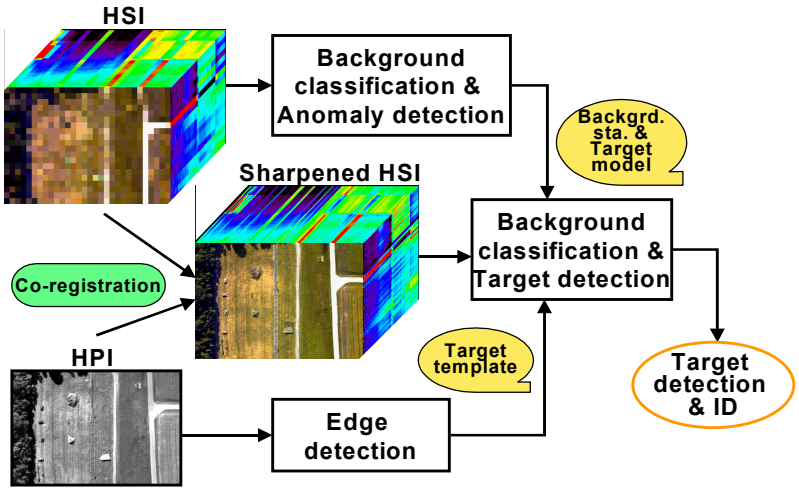

Figure5 A spatial-spectral analysis approach

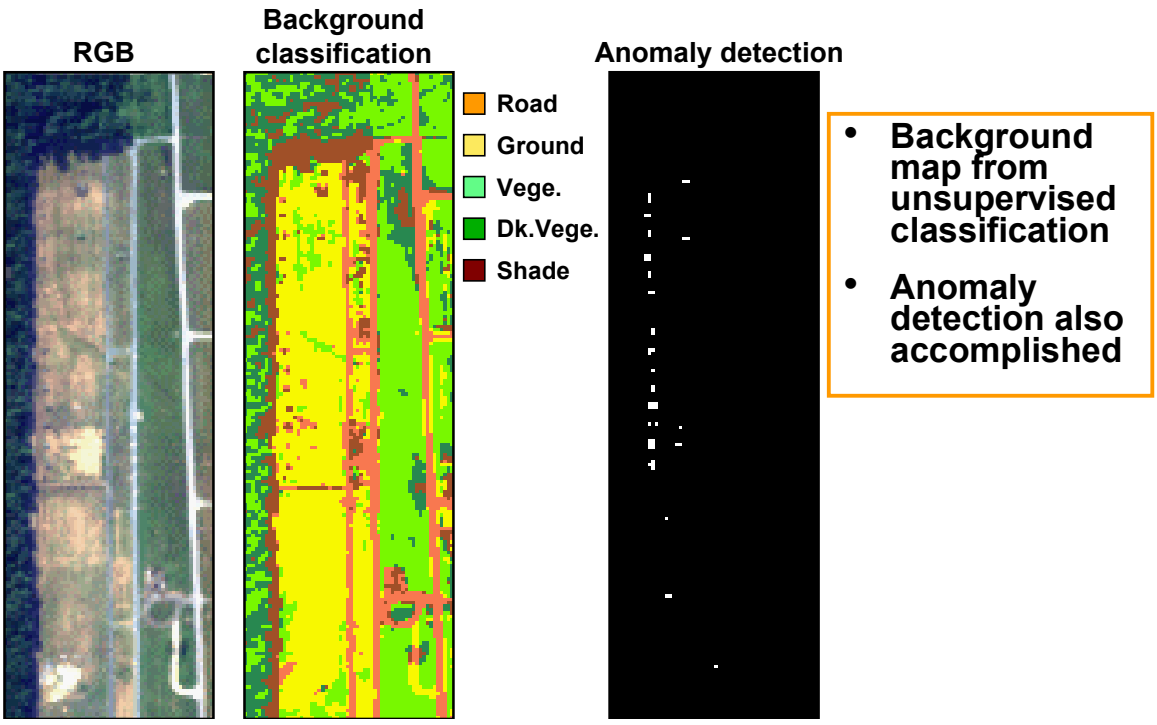

Figure 6 RGB image of HSI, background classification and anomaly detection derived also from the unsharpened HSI

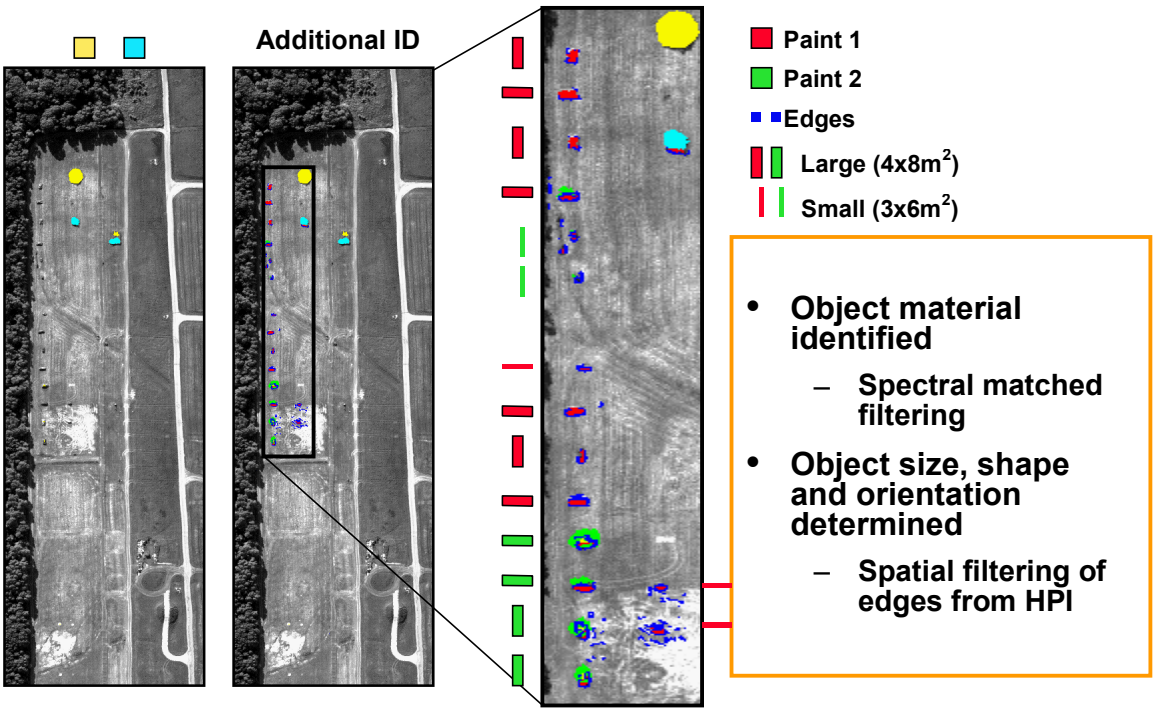

Figure 7 Fabric and additional object identification

4 Summary

HSI offers superior spectral resolution, and allows background characterization and material identification. It can be employed in conjunction with other remote sensing data to further enhance the overall system performance. In this paper, the potential of fusion of HSI with other sensors was illustrated. SAR compensated a disadvantage of HSI, such as lack of surface penetration due to passive sensing. Their sensing of different phenomenologies also helped in reduction of false alarm rates. Another shortcoming of HSI, due to tradeoff with rich spectral information, is sub-optimal spatial resolution. This can also be compensated by fusion with a broadband panchromatic imager, typically with much better spatial resolution.

Framework of HSI fusion with SAR and HPI was demonstrated. A common data set of P-3 SAR and HYDICE HSI from Dixie-97 data collection over Vicksburg, Mississippi was used for SAR/HSI fusion. Targets in the forest background included fabric nets and vehicles. Principal component analysis on HSI data was shown to allow effective spectral dimension reduction and feature extraction for terrain characterization and fabric net detection. SAR/HSI fusion was accomplished with a co-registration of the images using references to terrain features. The fusion results showed detection of a vehicle under a fabric net and a significant reduction of SAR false alarms due to trees. In addition, a case of SAR detection was confirmed by HSI with material identification of military vehicle paint.

For HSI/HPI data fusion, sharpening approaches were investigated and implemented on a combined HSI and HPI data set. The sharpened HSI retained the spectral signatures of extended area in HSI and in general appeared spatially sharper. However, spectral features of objects smaller than the original HSI resolution were not fully resolved through sharpening due to the under-determined nature of the combined data set. Further spatial and spectral analysis was then demonstrated to combine high-resolution information from HSI and HPI for enhanced background characterization and target detection and identification. Anomalies distinct from backgrounds were also detected from HSI and used to cue for target detection and identification in the combined analysis. Spatial image processing was applied to HPI for edge analysis. As a result of combined analysis, specific target material, size and shape were determined.

References

1. Schott, J. R., Remote Sensing, Oxford University Press, 1997
2. Tim J. Patterson, Michael E. Bullock, "Radiometrically Correct Sharpening of Multispectral Images using a Panchromatic Image", p. 252-264, SPIE Vol.2234
3. Tim J. Patterson, Lester Gong, Robert Haxton, Troy Chinen, "Extension of Sharpening Techniques to Hyperspectral Data", P. 114-122, SPIE Vol.3372, April 1998
4. Jim Vrabel, "Advanced Band Sharpening Study", p. 73-84, SPIE Vol.3071, April, 1997
5. Mark A. Goforth, "Multispectral Image Sharpening with Multiresolution Analysis and the MTF", P. 123-131, SPIE Vol.3372, April 1998
6. Harry N. Gross, John R. Schott, "Application of Spatial Resolution Enhancement and Spectral Mixture Analysis to Hyperspectral Images", P. 30-41, SPIE Vol.2821, 1996
7. Harry N. Gross, John R. Schott, "Application of Spectral Mixture Analysis and Image Fusion Techniques for Image Sharpening", P.85-94, Remote Sensing and Environment 63, 1998
8. Bing Zhang, Jiangui Liu, Xiangjun Wang, Changshan Wu, "Study on the Classification of Hyperspectral Data in Urban Area", P. 169-172, SPIE Vol.3502
9. S. M. Hsu, et al; “An Efficient Approach to Background Characterization of Hyperspectral images and Iits Applications”, Project Report HTAP-5, MIT Lincoln Laboratory, October 2000
10. R. C. Gonzalez, P. Wintz, Digital Image Processing, Addison-Wesley, 1987